

A novel 3D-QSAR comparative molecular field analysis (CoMFA) model of imidazole and quinazolinone functionalized p38 MAP kinase inhibitors

Gilberto M. Sperandio da Silva,^{a,b} Carlos M. R. Sant'Anna^{a,c} and Eliezer J. Barreiro^{a,b,*}

^aLaboratório de Avaliação e Síntese de Substâncias Bioativas (LASSBio), Faculdade de Farmácia, Universidade Federal do Rio de Janeiro (UFRJ), P.O. Box 68006, ZIP 21944-910, Rio de Janeiro, RJ Brazil

^bDepartamento de Farmacologia Básica e Clínica, Instituto de Ciências Biomédicas, Universidade Federal do Rio de Janeiro (UFRJ), Rio de Janeiro, RJ., Brazil

^cDepartamento de Química, ICE, Universidade Federal Rural do Rio de Janeiro (UFRRJ), Seropédica, RJ., Brazil

Received 28 March 2004; accepted 6 April 2004

Abstract—In this study we describe a new comparative molecular field analysis (CoMFA) model of dihydroquinazolinone and tetrasubstituted imidazole compounds with p38 MAPK inhibitory activity. A series of 51 (a training set of 40 and a test set of 11) dihydroquinazolinone [*Bioorg. Med. Chem. Lett.* **2003**, *13*, 277.] and tetrasubstituted imidazole [*J. Med. Chem.* **1999**, *42*, 2180.] derivatives known as p38 mitogen-activated protein kinase (p38 MAPK) selective inhibitors was studied by quantitative structure–activity relationship (3D-QSAR) analysis using comparative molecular field analysis. The 3D-QSAR models were generated and evaluated by a scheme that combines a genetic algorithm (GA) optimization with partial least squares (PLS) regression and by crossvalidation using the leave-one-out technique. The model was able to efficiently predict the activities of the compounds of the test set, suggesting that it can be used for the planning of new p38 MAPK inhibitor candidates useful to treat chronic inflammatory states.

© 2004 Elsevier Ltd. All rights reserved.

1. Introduction

MAP kinases are important signaling molecules that are activated by a number of extracellular stress stimuli. The events that are regulated by p38 MAPK lead to the production of cytokines such as tumor necrosis factor- α (TNF- α) and interleukin-1 β (IL-1 β).³ The TNF- α and IL-1 β are proinflammatory cytokines⁴ produced in response to infection and other sources of cellular stress. TNF- α inhibition has represented a fundamental role in the control of chronic inflammatory diseases such as rheumatoid arthritis.^{5–9}

Recently, research groups at Merck, Vertex, and Glaxo-SmithKline have implemented efforts to develop new lead compounds to selectively inhibit p38 MAPK, represented by compounds DQO-501 (1), VX-745 (2), SB203580 (3) (Fig. 1).^{1,3,10–15}

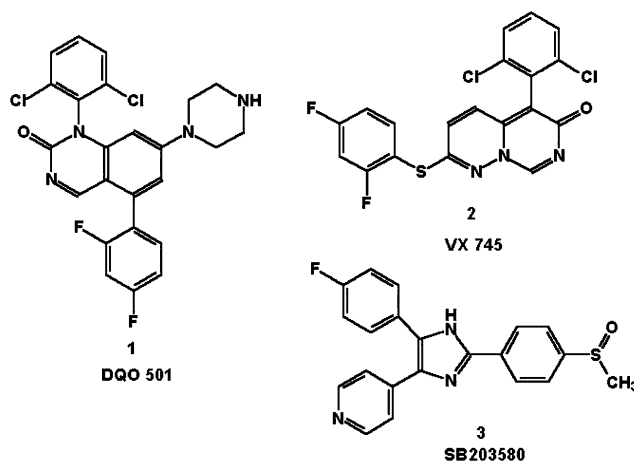


Figure 1. Recently discovered p38 MAPK inhibitors.

Keywords: CoMFA model; p38 Inhibitors; dihydroquinazolinone; Tetrasubstituted imidazole compounds.

* Corresponding author. Tel./fax: +552125626644;
e-mail: eliezer@ufrj.br

Quantitative structure–activity relationship (QSAR) is a methodology mostly used to correlate properties (such as biological activities) with chemical structures, but it can also be applied to predict the biological activity of nonsynthesized compounds structurally related to a training set of compounds. It is a statistically validated mathematical model of correlation between the chemical structures and their activity profiles.¹⁶ With the advent of molecular modeling, three-dimensional (3D) descriptors have replaced the traditional physicochemical and bidimensional descriptors.^{17–20}

Among the techniques of 3D-QSAR, comparative molecular field analysis (CoMFA)²¹ is now one of the most widely used techniques for the study of compounds with potential biological activity, as can be exemplified by studies on the development of selective inhibitors of the COX-2 enzyme as anti-inflammatory agents.^{22,23} The CoMFA method uses the Van der Waals steric (Lennard–Jones) and electrostatic (Coulomb) interaction energy descriptors, calculated with a probe charge over the 3D molecular surface. Statistical tools are used with the method, such as partial least-squares (PLS) analysis.

In the present paper, we describe a new CoMFA model for dihydroquinazolinone and tetrasubstituted imidazole compounds known as p38 MAPK selective inhibitors. The model was able to efficiently predict the biological activity of compounds not included in the training set, suggesting its potential for the planning of new candidates as p38 MAPK inhibitors.

2. Results and discussion

2.1. Statistical validation

2.1.1. Internal validation. Knowledge of the DQO-501 and SB203580 bioactive conformation obtained from the X-ray crystallographic inhibitor–enzyme complex and orientation suggested by Stelmach et al.¹ was of great importance in determining an experimentally derived alignment rule for the three training sets and their corresponding test sets.

The accuracy of actual predictions of the resulting QSAR can be determined through the value of the crossvalidated q^2 (crossvalidation correlation coefficient) reported by PLS. The statistical meaning of q^2 is different from that of the conventional correlation coefficient r^2 . A q^2 value greater than 0.3 is considered significant for the chance of significant correlation being <95%.^{24,25} Our results indicate the good predictive ability of the models, which yield high crossvalidated correlation coefficients q^2 values (from 0.846 to 0.876) with reasonable respective standard errors of prediction S_{cv} (from 0.326 to 0.384) (Table 1). The optimal number of components in each case, 5, is reasonable considering the number of compounds used to derive the models.

Table 1. Statistical results for the three CoMFA models

	Model 1	Model 2	Model 3
q^2 ^a	0.867	0.876	0.846
N ^b	5	5	5
S_{cv} ^c	0.379	0.384	0.326
r^2 ^d	0.865	0.836	0.878
S_e ^e	0.372	0.409	0.352
F ^f	58,775	40,338	58,287
r_{bs}^2 ^g	0.909	0.889	0.943
S_{bs} ^h	0.291	0.302	0.226
r_{pred}^2 ⁱ	0.740	0.919	0.542

^a Crossvalidation correlation coefficient.

^b Number of components.

^c Standard error of prediction.

^d Correlation coefficient.

^e Standard error of estimate.

^f F-ratio.

^g Bootstrapped correlation coefficient.

^h Bootstrapped standard deviation.

ⁱ Predicted correlation coefficient.

All three models were submitted to a leave-one-out crossvalidation using 40 compounds to predict the activity of the remaining 11. The results show that the q^2 values obtained for the three models with corresponding standard deviations are good and reliable (Table 1). No negative q^2 mean values were observed, which confirms the great internal consistency of our training sets. The three models yielded high conventional r^2 values (from 0.836 to 0.878) with reasonable standard errors of estimate s (from 0.352 to 0.409), as shown in Table 1. These data suggest a good correlation between the two molecular fields and the activities measured for the different compounds in the different models.

The confidence intervals (mean and standard deviation) for the parameters to be estimated can be calculated by a modern validation method, the bootstrap.²⁶ Both bootstrapping and crossvalidation involve repeatedly analyzing the actual data distribution. Bootstrapping provides confidence limits for various analysis parameters once the level of model complexity has been established, while crossvalidation tends to provide overall information, particularly about the level of model complexity appropriate with a particular analysis and dataset. Therefore, the bootstrapping provides an estimate of the variability of the parameters in a final model. The calculated variance of the parameter estimates reflects the accuracy with which any of the parameters can be estimated from the input data.²⁶ The high bootstrapped correlation coefficients (r_{bs}^2) (from 0.889 to 0.943) is indicative of a high degree of confidence in the analyses performed.

2.1.2. External validation. The three different training sets were then used to derive three separate CoMFA models taking into account the combination of the steric and electrostatic molecular fields. The predictive r^2 coefficients (r_{pred}^2) for the test set was calculated according to the following formula,

$$r_{\text{pred}}^2 = \frac{1 - \text{SSD}}{\text{PRESS}}$$

where SSD is the sum of squared deviation from the mean and PRESS is the sum of squared differences between the actual and the predicted values.²⁷ The r_{pred}^2 values are presented in Table 1. Among the three models constructed, the best predictive model was the second one ($r_{\text{pred}}^2 = 0.919$). The values of observed and calculated activities are given in Table 2. Additionally, model

Table 2. Calculated pIC50 values versus observed pIC50 values for the training and test sets of the best model

Compound	Observed	Training set		Test set	
		Calculated	gap	Calculated	gap
1a	5.68			6.52	−0.84
2a	5.85	6.60	−0.75		
3a	5.91	5.54	0.37		
4a	6.00	6.23	−0.23		
5a	6.01	6.28	−0.27		
6a	6.15			6.20	−0.05
7a	6.26	6.39	−0.13		
8a	6.31	6.67	−0.36		
1b	6.49	7.27	−0.78		
9a	6.52			6.46	0.06
10a	6.70	6.75	−0.05		
11a	6.74	6.72	0.02		
2b	6.77	7.01	−0.24		
12a	6.77	6.79	0.02		
13a	6.82			6.89	−0.07
14a	6.85	6.90	−0.05		
15a	6.86	6.84	0.02		
16a	6.89	6.84	0.05		
3b	6.89	6.75	0.14		
17a	6.92			7.45	−0.53
18a	7.07	7.19	−0.12		
4b	7.10	7.41	−0.31		
19a	7.15	7.76	−0.61		
5b	7.17	7.44	−0.27		
20a	7.32	6.61	0.71		
6b	7.33			7.53	−0.20
7b	7.36	7.47	−0.11		
8b	7.36	7.84	−0.48		
21a	7.41			7.18	0.23
22a	7.42	7.07	0.35		
23a	7.42	7.51	−0.09		
9b	7.52	7.52	0.00		
24a	7.55	6.72	0.83		
10b	7.66			7.66	0.00
25a	7.32	6.61	0.71		
11b	7.96	7.85	0.11		
12b	7.96	8.01	−0.05		
13b	7.96	7.84	0.12		
26a	8.05	7.96	0.09		
27a	8.12	8.04	0.08		
14b	8.15			8.11	0.04
15b	8.15	7.85	0.30		
28a	8.15	8.04	0.11		
16b	8.22	8.18	0.04		
17b	8.52	8.15	0.37		
29a	8.82			8.68	0.14
18b	9.00	8.05	0.95		
30a	9.01	9.09	−0.08		
31a	9.12	9.04	0.08		
32a	9.72			8.97	0.75
33a	9.96	10.13	−0.17		

2 has the best predictive capacity with a high crossvalidated correlation coefficient ($q^2 = 0.876$).

We compared the shapes of the electrostatic and steric CoMFA contours surrounding the tested molecules with the crystal structures of p38 MAPK in complex with SB203580 and DQO-501 as recovered from the Brookhaven Protein Data Bank. Graphic representations of the CoMFA model 2 are displayed in Figures 2 and 3. They show regions where variations of steric and electrostatic structural features of the different compounds of the training set lead to an increase or decrease in activity.

In order to analyze the steric contour plots of Model 2, the contour maps were compared with the topology of **14b** (a quinazolinone, series **b**) and **32a** (a tetrasubstituted imidazole, series **a**)-p38 MAPK complexes (Fig. 2). Only the residues within 5 Å around the inhibitors are shown for clarity. The color polyhedra in the maps surrounded all lattice points where the QSAR strongly associated changes in the compound field values with changes in their biological potencies. The steric contour plots of **14b** or **32a** are displayed as green contours, which indicate regions where an increase in steric bulk will enhance activity, and yellow contours, which indicate regions where an increase in steric bulk will reduce activity.²⁶ Therefore, the large region of yellow contour near the **14b** phenyl moiety suggests that there is an unfavorable steric region impairing the accessibility of the compound to the p38 MAPK active site. In fact, when the model was superimposed with p38 MAPK

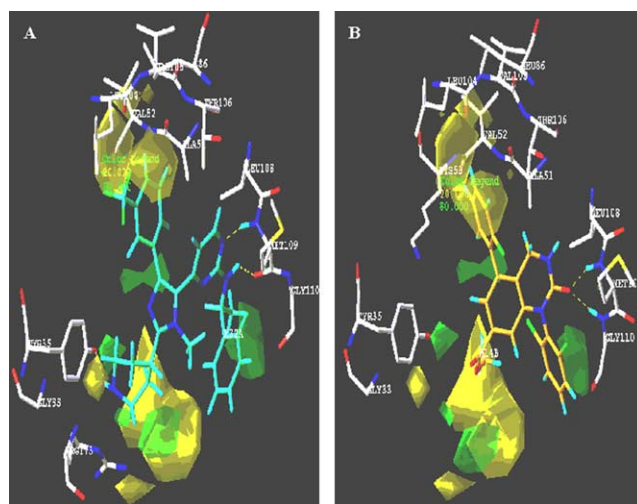


Figure 2. Contour maps of Model 2 as compared with the topology of **32a** and **14b**-p38 MAPK complex. Only the residues within 5 Å around the inhibitor are shown for clarity. The residues are represented as sticks, and the carbon atoms of the inhibitors are shown in green-blue (**32a**) or in orange (**14b**), blue (N), red (O), and green (halogen); the dashed lines are the hydrogen bonds formed between inhibitor and p38 MAPK. Steric contour plots of **32a** or **14b** are displayed in (A) and (B), respectively: green contours (>80% contribution) indicate regions where an increase in steric bulk will enhance activity, and yellow contours (<20% contribution) indicate regions where an increase in steric bulk will reduce activity.

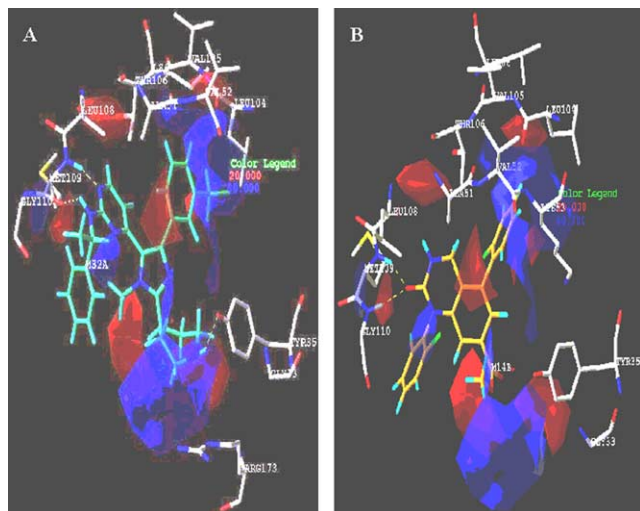


Figure 3. Contour maps of Model 2 as compared with the topology of **32a** and **14b**-p38 MAPK complex. Only the residues within 5 Å around the inhibitor are shown for clarity. The residues are represented as sticks, and the carbon atoms of the inhibitors are shown in green-blue (**32a**) or in orange (**14b**), blue (N), red (O), and green (halogen); the dashed lines are the hydrogen bonds formed between inhibitor and p38 MAPK. Electrostatic contour plots of **32a** or **14b** are displayed in (A) and (B), respectively: blue contours (>80% contribution) and red contours (<20% contribution) correspond to regions where an increase in positive or negative charge, respectively, will enhance activity.

hydrophobic pocket, it was observed that this yellow contour was near residue Leu104. On the other hand, the medium-sized green region, which is far from residues Ala111 and Gly110, could accommodate increased steric bulk that is associated with enhanced activity such as those of **14b** (represented by group F-phenyl of compound **14b**) or **32a** (represented by group NH-phenyl of compound **32a**). Small green contours near the piperidine (**32a**) moiety show that this group is associated with favorable steric regions (Fig. 2).

To analyze the electrostatic contour plots of Model 2, the contour maps were also compared with the topology of **14b**- and **32a**-p38 MAPK complexes (Fig. 3). The electrostatic contour plots are displayed in blue and red contours. The red areas are regions where negative potential is favorable to the inhibitory activity; the blue areas are regions where positive potential is favorable to the inhibitory activity. It is known that the peptidic N–H groups of residues Met109 and Gly110 could form hydrogen bonds with two important p38-inhibitors (1 and 14 E).¹ A red contour near the carbonyl group of **14b** quinazolinone moiety and NH **32a** piridinyl group indicates that electron-rich groups are beneficial to the inhibitory activity. This red polyhedra could be associated to the hydrogen bond with the N–H groups of residues Met109 and Gly110. Another red polyhedra near the NH group of **14b** quinazolinone moiety could also be associated with a hydrogen bond with residue Leu108 (Fig. 3). Additionally, the model shows a blue region near NH of the piperidine (**32a**) moiety that can be associated with residue Tyr35. The NH group could represent an important requisite for the activity of

piperidine derivatives since it is able to form a hydrogen bond with the O atom of the hydroxyl group of residue Tyr35. The measured distance of H (piperidine N–H) to the hydroxyl O atom of residue Tyr35, 2.25 Å, and N–H...O angle, 152.11°, are indicative of a hydrogen bond.

3. Conclusions

A series of 51 compounds of structurally different selective p38 tetrasubstituted imidazoles and dihydroquinazolinones MAPK inhibitors^{1,2} were used to generate and validate three 3D-QSAR models using CoMFA methodology. These three models were built using an alignment rule based on the orientation proposed by Stelmach and et al.¹ Model 2 was the best because it was the best predictive model ($r^2_{\text{pred}} = 0.919$) and had the best predictive capacity with a high cross-validated correlation coefficient ($q^2 = 0.876$). It was able to predict the inhibitory activities of 11 inhibitors of the p38 MAPK not included in the model construction and offers important structural insight for rational designing novel selective p38 MAPK inhibitors prior to their synthesis. Moreover, the model quality was also shown by a good correlation with the most important residues of the active site of p38 MAPK.

We conclude that the structural features indicated by this 3D-QSAR analysis may provide a helpful guideline to design novel compounds with inhibitory activities towards p38 MAPK.

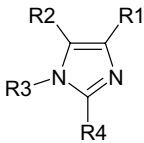
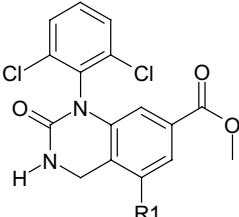
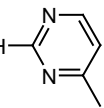
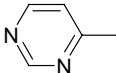
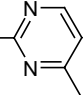
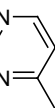
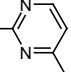
4. Experimental

4.1. Biological data

All inhibitory activity values of 51 compounds against the p38 MAPK were obtained with the same pharmacological protocol on the human recombinant enzyme in order to have consistent biological data, which was expressed in terms of pIC_{50} or $\log(1/\text{IC}_{50})$, where IC_{50} represents the drug concentration that inhibits 50% of the enzyme activity (Table 1).^{1,2} The inhibitors elected belong to two structurally different classes, tetrasubstituted imidazoles (series **a**: 33 compounds in Table 3)² and quinazolinones (series **b**: 18 compounds in Table 3).¹

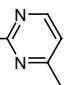
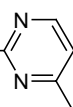
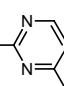
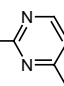
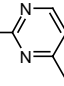
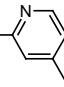
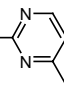
In Figure 4 it is shown that the enzyme inhibitory activities are widespread and homogeneous, which is a prerequisite if meaningful results are to be obtained from 3D-QSAR studies using the CoMFA method.¹⁶ Approximately 80% of the 51 compounds were subdivided into three individual training sets of 40 compounds each, and the remaining compounds, corresponding to approximately 20%, were used as test sets with 11 compounds each. The compounds were split between training and test sets at random. Random numbers were generated and assigned to each compound before they were sorted in increasing order. Then the three different training sets were used as the basis to construct three different CoMFA models and the com-

Table 3. Structures and p38 MAPK inhibitory activities of tetrasubstituted imidazoles (A) and quinazolinones (B) compounds

<div style="display: flex; justify-content: space-around; align-items: center;"> <div style="text-align: center;">  <p>Tetrasubstituted Imidazole (a: 33 compounds)</p> </div> <div style="text-align: center;">  <p>Quinazolinones (b: 18 compounds)</p> </div> </div>					
Compound	R ₁	R ₂	R ₃	R ₄	pIC ₅₀ Observed
1a	—i-C ₃ H ₇	4-C ₅ H ₄ N	H	C ₆ H ₅	5.68
2a	4-C ₆ H ₄ OH	4-C ₅ H ₄ N	H	C ₆ H ₅	5.85
3a	(s)-PhCH(CH ₃)NH- 	3-C ₆ H ₄ CF ₃	CH ₃	4-C ₅ H ₁₀ N	5.91
4a	4-C ₆ H ₄ C ₆ H ₅	4-C ₅ H ₄ N	H	C ₆ H ₅	6.00
5a	4-C ₆ H ₄ CN	4-C ₅ H ₄ N	H	C ₆ H ₅	6.01
6a	C ₆ H ₅		H	C ₆ H ₅	6.15
7a	3-C ₆ H ₄ OCH ₃	4-C ₅ H ₄ N	H	C ₆ H ₅	6.26
8a	3-C ₆ H ₄ F	4-C ₅ H ₄ N	H	C ₆ H ₅	6.31
1b	3-C ₆ H ₅ CH ₃	—	—	—	6.49
9a	4-C ₆ H ₄ OCH ₃	4-C ₅ H ₄ N	H	C ₆ H ₅	6.52
10a	4-C ₆ H ₅ CF ₃	4-C ₅ H ₄ N	H	C ₆ H ₅	6.70
11a	C ₆ H ₅	4-C ₅ H ₄ N	H	C ₆ H ₅	6.74
2b	3-C ₆ H ₅ CF ₃	—	—	—	6.77
12a	4-C ₆ H ₄ F	4-C ₅ H ₄ N	H	H	6.77
13a	2-C ₆ H ₄ Cl	4-C ₅ H ₄ N	H	C ₆ H ₅	6.82
14a	3-C ₆ H ₄ OH	4-C ₅ H ₄ N	H	C ₆ H ₅	6.85
15a	3,5-C ₆ H ₃ Cl ₂	4-C ₅ H ₄ N	H	C ₆ H ₅	6.86
16a	3-C ₆ H ₄ Cl	4-C ₅ H ₄ N	H	C ₆ H ₅	6.89
3b	4-CF ₃ -Phenyl	—	—	—	6.89
17a	C ₆ H ₅	H ₃ CNH- 	H	C ₆ H ₅	6.92
18a	3-C ₆ H ₅ CF ₃	4-C ₅ H ₄ N	H	C ₆ H ₅	7.07
4b	3-Fl-Phenyl	—	—	—	7.10
19a	4-C ₆ H ₄ F	4-C ₅ H ₄ N	H	C ₆ H ₁₁	7.15
5b	3-Cl-Phenyl	—	—	—	7.17
20a	4-C ₆ H ₄ Cl	4-C ₅ H ₄ N	H	C ₆ H ₅	7.32
6b	4-Cl-Phenyl	—	—	—	7.33
7b	4-CH ₃ -Phenyl	—	—	—	7.36
8b	2,6-di Fl-C ₆ H ₄	—	—	—	7.36
21a	4-C ₆ H ₄ F	4-C ₅ H ₄ N	H	4-C ₆ H ₄ SOCH ₃	7.41
22a	C ₆ H ₅	H ₂ N- 	H	C ₆ H ₅	7.42
23a	C ₆ H ₅	4-H ₃ COPhCH ₂ NH- 	H	C ₆ H ₅	7.42
9b	C ₆ H ₅	—	—	—	7.52
24a	3,4-C ₆ H ₄ Cl ₂	4-C ₅ H ₄ N	H	C ₆ H ₅	7.55
10b	4-Fl-Phenyl	—	—	—	7.66
25a	4-C ₆ H ₄ Cl	4-C ₅ H ₄ N	H	C ₆ H ₅	7.32
11b	2-CH ₃ -Phenyl	—	—	—	7.96

(continued on next page)

Table 3 (continued)

Compound	R ₁	R ₂	R ₃	R ₄	pIC ₅₀ Observed
12b	2,4-diFl-Phenyl	—	—	—	7.96
13b	2-CH ₃ -4-Fl-Phenyl	—	—	—	7.96
26a	4-C ₆ H ₄ F	4-C ₅ H ₄ N	H	4-C ₅ H ₉ NH	8.05
27a	3-C ₆ H ₄ CF ₃	4-H ₃ COPhCH ₂ NH- 	H	4-C ₅ H ₉ NH	8.12
14b	2-Fl-Phenyl	—	—	—	8.15
15b	2,4-di Fl-Phenyl	—	—	—	8.15
28a	3-C ₆ H ₄ CF ₃	H ₂ N- 	H	4-C ₅ H ₉ NH	8.15
16b	2-Cl-Phenyl	—	—	—	8.22
17b	2-Cl-4-F-Phenyl	—	—	—	8.52
29a	3-C ₆ H ₄ CF ₃	(R)-PhCH(CH ₃)NH- 	CH ₃	4-C ₅ H ₉ NH	8.82
18b	2-Cl-Phenyl	—	—	—	9.00
30a	3-C ₆ H ₄ CF ₃	(R)-PhCH(CH ₃)NH- 	H	4-C ₅ H ₉ NH	9.01
31a	3-C ₆ H ₄ CF ₃	(S)-PhCH(CH ₃)NH- 	H	4-C ₅ H ₉ NH	9.12
32a	3-C ₆ H ₄ CF ₃	(S)-PhCH(CH ₃)NH- 	CH ₃	4-C ₅ H ₉ NH	9.72
33a	3-C ₆ H ₄ CF ₃	(S)-PhCH(CH ₃)NH- 	H	4-C ₅ H ₉ NH	9.96

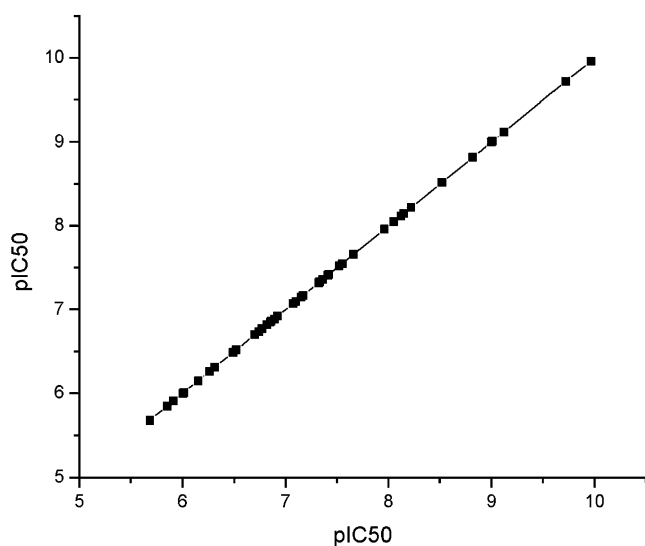


Figure 4. Distribution of inhibitory activities (pIC₅₀) of 51 compounds against the p38 MAPK are widespread and homogeneous, which is a prerequisite if meaningful results are to be obtained from 3D-QSAR studies using the CoMFA method.

pounds of the three test sets were used for model validation.

4.2. Molecular modeling

The crystal structures of p38 MAPK in complex with two inhibitors, DQO-501 (**1**) and SB203580 (**3**) (Fig. 5), were recovered from the Brookhaven Protein Data Bank (<http://www.rcsb.org/pdb/>) (entry codes 1A9U and 1M7Q, respectively). The conformation and orientation in space of DQO-501 (**1**) and SB203580 (**3**) extracted from the X-ray crystallographic inhibitor–enzyme complexes were used as templates for the construction of compounds from series *a* and series *b*, respectively, assuming that these conformations represent the most probable bioactive conformations of the compounds at the enzyme active site level. The initial structures of the 51 compounds were generated by the molecular modeling software SYBYL 6.8.²⁶ The geometries of these compounds were subsequently optimized using the Tripos force field with Gasteiger–Hückel charges.²⁶ The

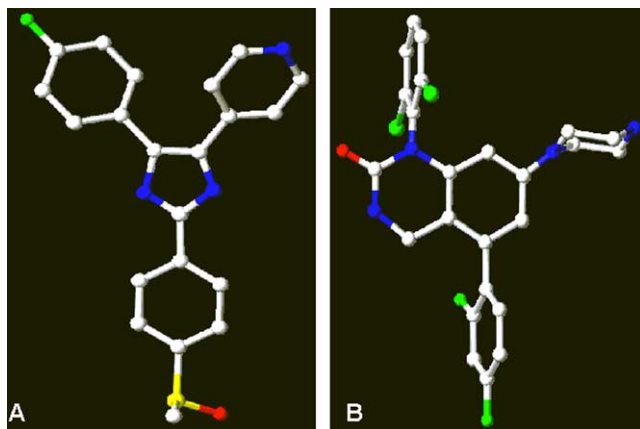


Figure 5. The conformation and orientation in space of Sb-203580 (A) and DQO-501 (B) extracted from the X-ray crystallographic inhibitor–enzyme complexes. Crystal structures of p38 MAPK in complex with Sb-203580 (A) and DQO-501 (B) were recovered from the Brookhaven Protein Data Bank (<http://www.rcsb.org/pdb/>) (entry codes 1A9U and 1M7Q, respectively). Color code: gray (C), blue (N), red (O), yellow (S), and green (halogen).

Powell method available in the Maximin2 module of SYBYL 6.8²⁶ was used for energy minimization with an energy convergence gradient value of 0.001 kcal/(mol Å).

4.3. Criteria for compound alignment

The conformation and orientation of the SB203580 (3) imidazole moiety (Core 1, the common substructure to all imidazole molecules, Figure 6) was used for superposition of the 33 tetrasubstituted imidazoles (series *b*). The molecules of series *a* were aligned using the database alignment method in SYBYL. After alignment of the molecules, the most active molecule of series *b* (**18b**) was added to the common database through manual alignment based on the orientation proposed by Stelmach and et al.¹ The three main atoms of series *a* and the three main atoms of series *b* served as a base for the

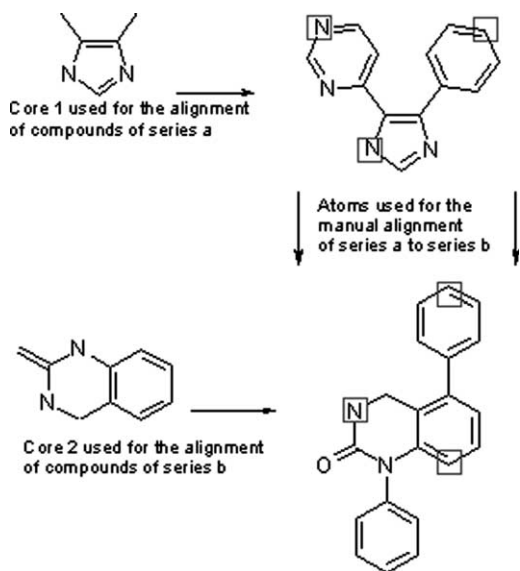


Figure 6. Strategy used to superposition of compounds of series *a* and series *b*.

union of the two families of compounds. For the alignment of the other molecules of series *b*, the conformation and orientation of the **32a** quinazolinone moiety (Core 2, the common substructure to all quinazolinone molecules, Figure 6) was used for superposition of the other 17 quinazolinone derivatives. Finally, these molecules were aligned using the database alignment method of SYBYL. An example of this alignment is presented in Figure 7.

5. D QSAR/CoMFA analysis

The CoMFA method was applied to the alignments provided by the SYBYL program (QSAR module) for the 3D QSAR analysis. The steric (Lennard–Jones) and electrostatic (Coulomb) CoMFA fields were calculated at all intersections in a regularly spaced (1.5 Å) grid

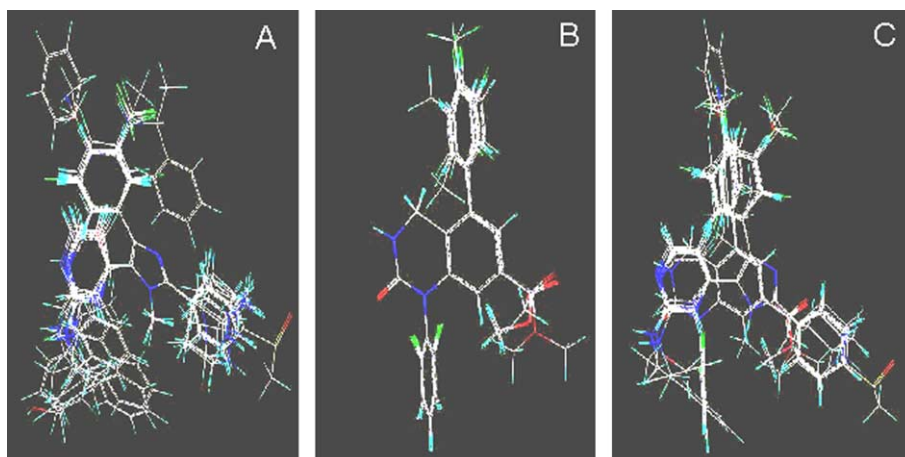


Figure 7. (A) Superposition of compounds of series *a*. (B) Superposition of compounds of series *b*. (C) Superposition and final alignment proposed of compounds used in this study.

within a predefined region. The steric and electrostatic interaction energies between a probe atom and the molecules were calculated using an sp^3 carbon as the steric probe atom and a +1.00 charge for the electrostatic probe. A cutoff of 5 kcal/mol was adopted, and the regression analysis was carried out using the full cross-validated partial least squares (PLS)^{28,29} method (leave-one-out) with CoMFA standard options for scaling of variables. To perform the PLS, the minimum column filtering value was set to 4.0 kcal/mol to improve the signal-to-noise ratio by omitting those lattice points whose energy variation was below this threshold and the number of components was set to 5.

Acknowledgements

We gratefully acknowledge financial support provided by CNPq (grants 52.1118/01-8; 50.0185/2003-4; BR.), PRONEX (0888; BR.), FAPERJ (E-26/152.172/2002; BR.) and fellowships (to E.J.B. and C.M.R.S.) from CNPq (BR.).

References and notes

- Stelmach, J. E.; Liu, L.; Patel, S. B.; Pivnichny, J. V.; Scapin, G.; Singh, S.; Hop, C. E.; Wang, Z.; Strauss, J. R.; Cameron, P. M.; Nichols, E. A.; O'Keefe, S. J.; O'Neill, E. A.; Schmatz, D. M.; Schwartz, C. D. *Bioorg. Med. Chem. Lett.* **2003**, *13*, 277.
- Liverton, N. J.; Butcher, J. W.; Claiborne, C. F.; Claremon, D. A.; Libby, B. E.; Nguyen, K. T.; Pitzenger, S. M.; Selnick, H. G.; Smith, G. R.; Tebben, A.; Vacca, J. P.; Varga, S. L.; Agarwal, L.; Dancheck, K.; Forsyth, A. J.; Fletcher, D. S.; Frantz, B.; Hanlon, W. A.; Harper, C. F.; Hofsess, S. J.; Kostura, M.; Lin, J.; Luell, S.; O'Neill, E. A.; Orevillo, C. J.; Pang, M.; Parsons, J.; Rolando, A.; Sahly, Y.; Visco, D. M.; O'Keefe, S. J. *J. Med. Chem.* **1999**, *42*, 2180.
- Lee, J. C.; Laydon, J. T.; McDonnell, P. C.; Gallagher, T. F.; Kumar, S.; Green, D.; McNulty, D.; Blumenthal, M. J.; Heys, J. R.; Landvatter, S. W.; Strickler, J. E.; McLaughlin, M. M.; Siemens, I. R.; Fisher, S. M.; Livi, G. P.; White, J. R.; Adams, J. L.; Young, P. R. *Nature* **1994**, *372*, 739.
- Koj, A. *Biochim. Biophys. Acta* **1996**, *1317*, 84.
- Elliott, M. J.; Maini, N. M.; Feldmann, M.; Kalden, J. R.; Antoni, C.; Smolen, J. S.; Leeb, B.; Breedveld, F. C.; Macfarlane, J. D.; Bijl, H.; Woody, J. N. *Lancet*. **1994**, *344*, 1105.
- Elliott, M. J.; Maini, N. M.; Feldmann, M.; Long-Fox, A.; Charles, P.; Bijl, H.; Woody, J. N. *Lancet*. **1994**, *344*, 1125.
- Rankin, E. C. C.; Choy, E. H. S.; Kassimos, D.; Kingsley, G. H.; Sopwith, A. M.; Isenberg, D. A.; Panayi, G. S. *Br. J. Rheumatol* **1995**, *34*, 334.
- Van Dulleken, H. M.; Van Deventer, S. J. H.; Hommes, D. W.; Bijl, H.; Jansen, J.; Tytgat, G. N. J.; Woody, J. N. *Gastroenterology* **1995**, *109*, 129.
- Moreland, L. W.; Baumgartner, S. W.; Schiff, M. H.; Tindall, E. A.; Fleischmann, R. M.; Weaver, A. L.; Ettlinger, R. E.; Cohen, S.; Koopman, W. J.; Mohler, K.; Widmer, M. B.; Bloesch, C. M. *N. Engl. J. Med.* **1997**, *337*, 141.
- Badger, A. M.; Bradbeer, J. N.; Votta, B.; Lee, J. C.; Adams, J. L.; Griswold, D. E. *J. Pharmacol. Exp. Ther.* **1996**, *279*, 1453.
- Hanson, G. H. *Exp. Opin. Ther. Patents* **1997**, *7*, 729.
- Salituro, F. G.; Germann, U. A.; Wilson, K. P.; Bemis, G. W.; Fox, T.; Su, M. S. *Curr. Med. Chem.* **1999**, *6*, 807.
- Salituro, F.; Bemis, G.; Cochran, J. Intl. Patent WO 99/64,400, 1999.
- Boehm, J. C.; Adams, J. L. *Exp. Opin. Ther. Patents* **2000**, *10*, 25.
- Dumas, J.; Sibley, R.; Reidl, B.; Monahan, M. K.; Lee, W.; Lowinger, T. B.; Redman, A. M.; Johnson, J. S.; Kingery-Wood, J.; Scott, W. J.; Smith, R. A.; Bobko, M.; Schoenleber, R.; Ranges, G. E.; Housley, T. J.; Bhargava, A.; Wilhelm, S. M.; Shrikhande, A. *Biorg. Med. Chem. Lett.* **2000**, *10*, 2047.
- Kubinyi, H. In *QSAR: Hansch Analysis and Related Approaches. Methods and Principles in Medicinal Chemistry*; Mannhold, R., Krogsgaard-Larsen, P., Timmerman, H., Eds.; VHC: Weinheim, 1993.
- Chen, J. Z.; Hu, L. H.; Jiang, H. L.; Gu, J. D.; Zhu, W. L.; Chen, Z. L.; Chen, K. X.; Ji, R. Y. *Bioorg. Med. Chem. Lett.* **1998**, *8*, 1291.
- Debnath, A. K. *J. Chem. Inf. Comput. Sci.* **1998**, *38*, 761.
- Jung, M.; Kim, H. *Bioorg. Med. Chem. Lett.* **2001**, *11*, 2041.
- Verli, H.; Albuquerque, M. G.; Alencastro, R. B.; Barreiro, E. J. *Eur. J. Med. Chem.* **2002**, *37*, 219.
- Cramer, R. C.; Patterson, D. E.; Bunce, J. D. *J. Am. Chem. Soc.* **1988**, *110*, 5959.
- Chavatte, P.; Yous, S.; Marot, C.; Baurin, N.; Lesieur, D. *J. Med. Chem.* **2001**, *44*, 3223.
- Liu, H.; Huang, X.; Shen, J.; Luo, X.; Li, M.; Xiong, B.; Chen, G.; Shen, J.; Yang, Y.; Jiang, H.; Chen, K. *J. Med. Chem.* **2002**, *45*, 4816.
- Cho, S. J.; Tropsha, A. *J. Med. Chem.* **1995**, *38*, 1060.
- Akamatsu, M. *Curr. Top. Med. Chem.* **2002**, *2*, 1381.
- SYBYL, Version 6.8. Tripos Associates: St. Louis, MO, 2001.
- Avery, M. A.; Muraleedharan, K. M.; Desai, P. V.; Bandyopadhyaya, A. K.; Furtado, M. M.; Tekwani, B. L. *J. Med. Chem.* **2003**, *46*, 4244.
- Weiner, S. J.; Kollman, P. A.; Case, D. A.; Singh, C.; Ghio, G.; Alagona, S.; Profeta, P.; Weiner, P. J. *Am. Chem. Soc.* **1984**, *106*, 765.
- Ghose, A. K.; Viswanadhan, V. N.; Wendoloski, J. J. *J. Comb. Chem.* **1999**, *1*, 55.